

## Sensorless control of permanent magnet synchronous generator drive using reduced switch inverter

### Sürekli mıknatıslı senkron generatörün azaltılmış anahtarlı evirici ile sensörsüz kontrolü

Ömer Cihan KIVANÇ<sup>1</sup>, Salih Barış ÖZTÜRK<sup>2</sup>

<sup>1,2</sup>Electrical and Electronics Engineering, Faculty of Engineering, Okan University, Tuzla, Istanbul, Turkey.  
cihan.kivanc@okan.edu.tr, baris.ozturk@okan.edu.tr

Received/Geliş Tarihi: 17.05.2017, Accepted/Kabul Tarihi: 25.04.2018

\* Corresponding author/Yazışılan Yazar

doi: 10.5505/pajes.2018.94770

Research Article/Araştırma Makalesi

#### Abstract

The main aim of this paper is to provide electric power generation using a renewable and portable method in rural and geographically problematic areas where energy transmission is not possible. Electric power generation from wind with low-cost, efficient and portable small-scale wind turbine during natural disasters (earthquake, fire, flood, etc.) leading to catastrophic consequences (long electrical black-outs) and for individual low power applications is targeted. The control of gearless Permanent Magnet Synchronous Generator (PMSG) along with load side inverter control in this project are performed using a full-rating, bi-directional, two-level, back-to-back voltage source rectifier/inverter with total of eight switches for the variable speed wind turbine. Additionally, one of the major advantages and novelty of using MRAS rotor flux linkage and stator resistance estimator in this system is to correct changes in the flux and stator resistance values in the control system. Due to its simplicity and effectiveness, the load side control is achieved by using four switch grid side inverter. To observe the total system performance, a three-phase passive load is used at the inverter output. The low-pass LCL filter is designed and used in the load side to reduce current and voltage harmonics and increase stability and efficiency of the power network. The results of the overall system are validated with the real-time DSP system. It is proved with this paper that the inclusion of a simple, effective and economical position sensorless control in the generator side show that renewable wind energy system can be a viable distributed green energy solution for rural areas.

**Keywords:** MRAS, Feedforward voltage estimation, PMSG, Four switch three phase inverter (FSTPI)

#### Öz

Bu makalenin temel amacı, enerji iletiminin mümkün olmadığı kırsal ve coğrafi açıdan problemlili bölgelerde yenilenebilir ve taşınabilir bir şekilde elektrik enerjisi üretimini sağlamaktır. Önerilen sistem ile katastrofik sonuçları (uzun süreli ve yerel olmayan elektrik kesintisi) olan doğal felaketler (deprem, yangın, sel vb.) sırasında düşük fiyata, verimli ve taşınabilir küçük ölçekli rüzgar türbini ve tahrik sistemi ile rüzgardan bireysel düşük güçlü elektrik enerjisi üretimi hedeflenmektedir. Bu çalışmada, redüktörsüz sürekli mıknatıslı senkron generatörün (SMSG) yük tarafı evirici kontrollü değişken hızlı rüzgar türbini için toplam sekiz anahtarlama elemanlı, tam yükünde çalışabilen, iki yönlü, iki seviyeli, sırt sırta bağlı gerilim kaynaklı doğrultucu/evirici kullanılarak gerçekleştirilir. Ayrıca, bu sistemde model referans adaptif sistem (MRAS) ile rotor kaçak akısı ve stator direnci kestirimcisi kullanılmasının en önemli avantajlarından birisi ve yeniliği, kontrol sistemindeki akı ve stator direnç değerlerinde meydana gelen değişikliklerinden kaynaklı bozulmaları düzeltmektedir. Basitliği ve etkin çalışma aralığı nedeniyle yük tarafının kontrolü dört anahtarlı şebeke tarafı eviricisi ile gerçekleştirilmiştir. Toplam sistem performansını gözlemlemek için evirici çıkışında üç fazlı pasif bir yük kullanılmaktadır. Akım ve gerilim harmoniklerini azaltmak, güç şebekesinin kararlılığını ve verimliliğini artırmak için yük tarafında alçak geçiren LCL filtre tasarlanmıştır ve gerçekleştirilmiştir. Bütün sistemin performansı gerçek zamanlı Sayısal İşaret İşleyici (Sİİ) sistemi ile doğrulanmıştır. Bu makalede, generatör kontrolü için geniş çalışma aralığı ve ekonomik pozisyon sensörsüz kontrolün dahil edilmesi ile yenilenebilir rüzgar enerjisi sisteminin kırsal alanlar için uygulanabilir bir dağıtık yeşil enerji çözümü olabileceği gösterilmektedir.

**Anahtar kelimeler:** MRAS, İleri beslemeli gerilim tahmini, SMSG, Dört anahtarlı üç fazlı inverter

## 1 Introduction

The difference between fossil energy sources and demanded energy needs is rapidly increasing. This leads to a search for alternative solutions in energy production. These solutions encourage utilizing the existing sources most efficiently. While the macro-scale systems meet existing needs in industrial and high power level practices, participating of individual users in energy production is possible with micro-scale systems [1]-[4]. Especially in rural areas, base stations, highways where the electricity cannot be delivered and individual usages are considered as micro-scale energy production application areas [5]. With the integration of smart grids, it is predicted that there may be a rapid increase in small energy production. In renewable energy production, the largest production share except hydroelectric power plants is provided from wind turbines. With the standard three-blade wind turbine structure,

both micro and macro levels of energy are produced. Small wind market share was \$ 60 million in the USA in 2014. In the "Small Wind Turbines" report prepared in 2010, unit, market and power capacity are analyzed. According to the report, it is stated that the number of units decreased 20%, the total power capacity increased 26% and market share increased 53% when compared to the previous year [1],[2]. It is stated that in England electricity generation reached to 1.84 MW capacity in 2013 based on wind energy in which the power range is between 0 and 1.5 kW [4]. To get the maximum use of wind energy, variable speed generators that can operate at a wide speed range are widely used in industry. With variable speed power generation, it is possible to obtain the maximum power at variable wind speeds [6]. By adjusting the generator speed at different working points according to speed-power characteristics of wind turbines, the maximum power point is obtained. In variable speed wind turbines systems, PMSG and

induction generator (IG) are commonly used [7]-[11]. PMSG is used in small turbine systems due to its high-power density, high efficiency and reliable design. The turbine connection of PMSG can be performed with or without a gear-box [12],[13]. However, because of cost, reliability and maintenance needs, a gear-box is not used in small powered systems. In variable-speed PMSGs, rotor rotational speed and wind speed are known with the position sensors and anemometer, respectively. However, in order to increase the robustness and reliability of the system, sensorless control methods are applied in PMSG [14]. Thus, maintenance needs and complex connections and assembly resulting from the usage of sensors are eliminated. In the proposed system, sensorless control method based on the principle of feedforward stator voltage estimation is suggested for maximum power output of direct drive PMSG. The rotor flux linkage and stator resistance available at generator steady-state equations are predicted on-line with MRAS observer in order to prevent the loss of positioning accuracy caused from parameter changes and then the updates are performed in the feedforward voltage estimation (FFVE) equations [12],[15]. Field-oriented control (FOC) and DTC technique need the accurate electrical parameters of the PMSM [13]. The least-square method slows down the processor too much because it has a repetitive process structure. Sliding-mode control (SMO) is used as an adaptive control method which is superior under parameter uncertainties [16],[17]. Similarly, an on-line parameter identification method uses extended-EMF method for more accurate position estimation [18]. In PMSG, rotor flux linkage undergoes a change during operation depending on the magnetic properties of the magnets and temperature rise [19]. The proposed method suggested by Okuyama et al. [15] is called the Flux-Vector control in which a PI controller is employed on the flux component of the current for IM. Additionally, one of the main advantages of this method is the elimination of voltage feedback. In the proposed feedforward voltage estimation method, flux change affects the control system and stability [20]. In the proposed method, when compared to other position sensorless control algorithms, since the speed is predicted primarily, the rotor position is obtained afterwards with the help of a simple integration and first degree low pass filter without any derivative term [15],[21],[22]. In the proposed small wind turbine control system, PMSG control is developed by using an inverter/rectifier structure in a back-to-back, bi-directional and reduced switching structure for variable speed wind turbines. In this topology, four of the switches form the three-phase two-leg system in the generator side and the other four are also used as three-phase two-leg system in the grid (off-grid) side [23]-[27]. Third phase leg of both circuits are connected to the center tap of the DC-link capacitors. Although in PMSG control systems, a structure containing twelve switches is often used, because the proposed method is for low power and for individual use, the elements increasing the cost are reduced [23]-[27]. With the MPPT method, power generation with optimum tip-speed ratio is obtained. In this study, two four-switch converter structures are established with two DC-link capacitors between them [23]-[27]. By keeping the  $d$ -axis current as zero using a PI regulator which is in the generator side of the rectifier, maximum electrical torque production is achieved. The MPPT method is used in order to obtain the maximum output power depending on optimum rotor speed under variable wind speeds.

The principle of proposed control algorithm is presented in Section 2. In Section 3, the proposed speed sensorless control scheme based on MRAS has been implemented with 1 kW PMSG drive controlled by a TMS320F28335 DSP. The hardware implementation and experimental results of the proposed sensorless PM synchronous generator drive including steady-state load disturbance are presented and discussed.

## 2 Proposed control algorithm

### 2.1 Principle of feedforward voltage estimation

The stator voltage equations of the IPMSM in the rotating  $dq$  reference frame are given by Equation (1) and (2), omitting the influences of magnetic field saturation and magnetic hysteresis as,

$$v_q = R_s + L_q \frac{di_q}{dt} + (\omega i_q L_d + \omega \lambda_{dr}) \quad (1)$$

$$v_d = i_d R_s + L_d \frac{di_d}{dt} - \omega i_q L_d \quad (2)$$

Where  $v_d, v_q, i_d, i_q$  are the stator  $dq$ -axes voltages and currents, respectively;  $R_s$  is the stator resistance;  $L_d$  and  $L_q$  represent the  $dq$ -axes inductances;  $\omega$  denotes the rotor angular electrical speed; and  $\lambda_{dr}$  is the rotor flux linkages [28]-[30]. In stator voltage estimation, stator resistance is controlled depending on the error between reference  $d$ -axis current and feedback  $d$ -axis current. The reason why the method has high and dynamic control capability is that resistance change does not affect it very much. Moreover,  $q$ -axis current is controlled by speed feedback. The method used in this paper is similar to the method proposed by Okuyama which was applied to induction machine. The proposed method is based on the PM (permanent magnet) synchronous machine parameters, therefore both stator resistance and magnet flux are estimated by an observer and updated online. According to the method based on stator voltage estimation, the voltage signal is added to  $v_q$  as a feedforward signal. In speed estimation,  $\Delta v$  is taken as the reference which varies proportional to speed. In the proposed method, while the stator resistance change effects are not taken into consideration continuously, the rotor flux linkage variation determines the performance of the proposed control method. The rotor flux linkage is controlled by an additional feedforward voltage signal.  $K$  value is a gain which is determined based on the variable speed zone. Start-up performance of the generator relies on  $K$  value that should be fixed properly as an important parameter in the proposed sensorless control. The proposed feedforward voltage estimations are given as,

$$v_q^* = i_q^* \hat{R}_s + (\omega_e L_d i_d^* + \omega_e \hat{\lambda}_f) + K \Delta v \quad (3)$$

$$v_d^* = i_d^* \hat{R}_s - \omega_e L_q i_q^* + \Delta v \quad (4)$$

Where  $\Delta v$  is the output of the  $d$ -axis PI current regulator and  $\omega_e$  is the output of the  $q$ -axis PI current regulator.  $\Delta v$  is multiplied by gain  $K$  and added to the  $q$ -axis voltage equation  $v_q^*$  representing the part of the derivative term in the dynamic voltage equation given in Equation (3). Similarly, the  $\Delta v$  terms in Equation (3) and Equation (4) also behave as the derivative representation given in Equation (1) and Equation (2) for achieving a better transient response in the sensorless operation. The  $dq$  frame stator voltages given in Equation (3) and (4) are obtained by modifying the dynamic machine model

and used as the basic reference signals to control the PM generator without requiring a position sensor. The signals depend on generator parameters. At any operating point, the machine itself determines the required voltages at its terminal by letting the inverter duplicate the voltages. This process is so-called as self-control.

### 2.2 Principle of four-switch inverter topology and LCL output harmonic filter design

There are only four active non-zero and no zero voltage vectors in a conventional FSTP inverter. Once all the transformations are kept the same, there are only three possible voltage space vector combinations in the stationary reference frame, as shown in Figure 1, when phase-*a*, is fixed to the center-tap of the DC-bus capacitors. If the conventional transformations in a six-switch inverter are used, only phase-*a* that is connected to the center-tap will make all non-zero voltage space vectors align with  $\alpha\beta$ -plane for FSTP inverter that is shown in Figure 1.

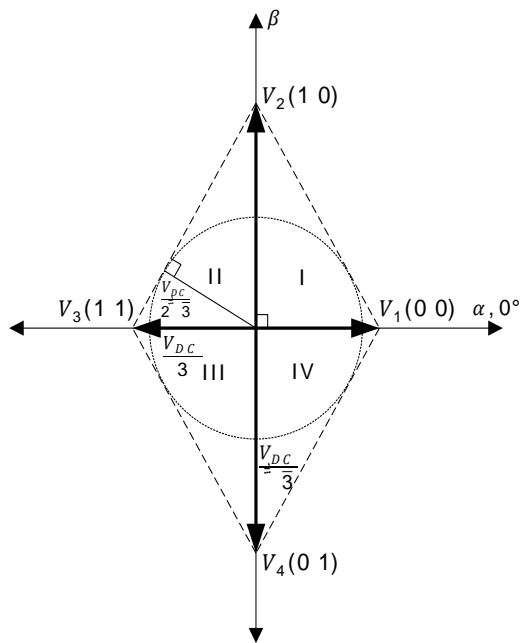


Figure 1: Voltage vectors of FSTP VSI in  $\alpha\beta$ -axes when phase-*a* is attached to the center-tap.

Once the voltage vectors are aligned with the  $\alpha\beta$ -axes, there is a simple and effective way to determine the sectors by monitoring the already available  $\alpha\beta$ -axes voltage vector references in digital controller without requiring estimated position data if the position sensor is not used in the control. If an actual rotor position is used to determine the sectors, all of the three possible phase connections to the center-tap will be sufficient to obtain the correct sectors. However, if the rotor position is estimated rather than measured as in this paper, any small error in the estimated rotor position degrades the performance of the drive when determining the correct sectors by position data in the FSTP inverter. In the proposed simple method, on the other hand, the  $\alpha$ - and  $\beta$ - axes voltage signals are readily available in the controller with no extra sensors like voltage sensors. The switching order is illustrated in Figure 1 when phase-*a* is attached to the center-tap, phase-*b* is connected to the middle leg and phase-*c* is fixed to the remaining leg of the inverter. In Figure 2, grey parts denote the on states of the corresponding switches and the white colored sections are the off states. As it is seen in Figure 2 that in each

sector, the zero-voltage vector effect is formed by using two short vectors  $V_1(0 0)$  and  $V_3(1 1)$  in equal amount  $T_0/2$  because the long vectors generate larger voltage drop on inductive loads and generates larger ripples.

The inverter located on the load/grid side transmits the current/voltage that contains a large number of harmonics due to high frequency PWM signals [31]. With a harmonic filter that can be located between inverter and load/network, the harmonics that would be transmitted to load/grid are greatly reduced and voltage and current waveforms in low THD (Total Harmonic Distortion) values close to pure sine are obtained [32]. Harmonic filters can also prevent the possible short circuit that can arise in the direct connection stage between two sources (inverter and load/grid) as well as decreasing high frequency harmonics. These harmonics diminishing techniques can be classified under the main approach of magnetic flux compensation, multilevel inverter, active and passive filtering.

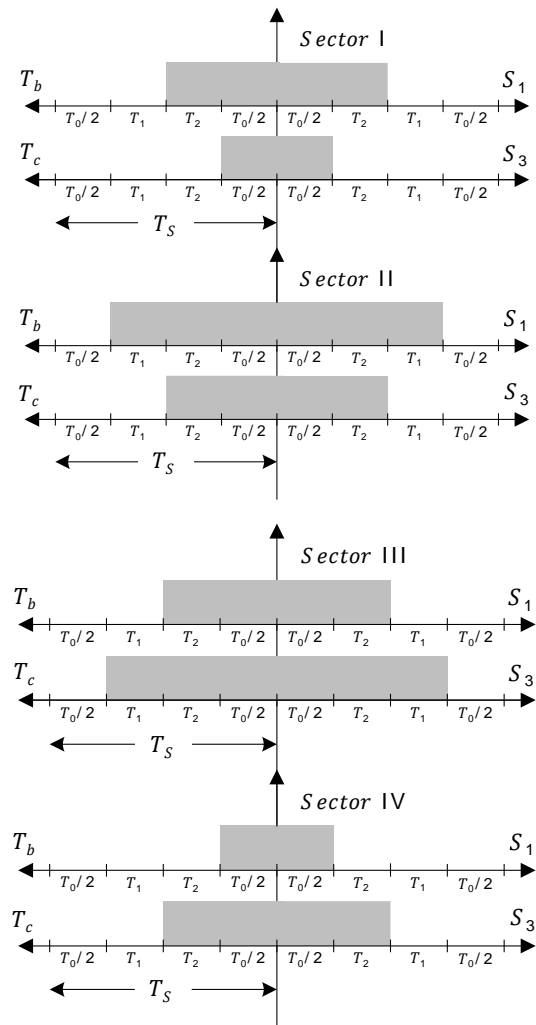


Figure 2: Switching sequence for Sector I and II, Sector III and IV.

In order to diminish the current harmonics around the switching frequency and to conform to standards like IEEE 519-1992, IEEE 1547-2008, IEEE 929-2000, IEC 61000-3 and IEC 61727, a low pass passive filter is used between inverter output and grid/load [33]. Ideally, a filter that has high damping attenuation in the lower cut-off frequency and high switching frequency can diminish the fluctuation occurring in the

switching frequency, significantly. In passive filter design, the issues such as switching loss, efficiency, voltage drop and stability (the system's entering into resonance) must be considered. For example, in the inverter systems operating synchronized to grid, IEEE standards state that each current harmonic above 35<sup>th</sup> harmonic must be less than 0.3% of rated current in the fundamental frequency. In industry and literature, L, LC and LCL type filters and their various derivatives are used in the inverter output [34]. The third degree low pass LCL-filter weakens the harmonics better in the switching frequency of the inverter than the other two filters mentioned above. LCL-filter provides better coupling impedance between grid/load and the filter [35]. Because the high harmonics will be absorbed by shunt capacity, it will receive much less ripple current on the  $L_2$  inductance in the side of grid/load and that's why it will enable this inductance to be selected smaller than  $L_1$  inductance in the inverter side input. LCL-filter provides good harmonic weakening even with small  $L$  and  $C_f$  values. However, it is necessary to address the problems of resonance effect, current ripple that may occur in inductances, total filter impedance, attenuation of current harmonics that may occur in switching frequency and around it and the amount of reactive power that is absorbed by capacity in LCL-filter design [36].

A parallel suppressor resistor has been inserted to the shunt capacitor used in LCL-filter. The reason of this process is the harmonic declination in characteristic resonance frequency. Figure 3 demonstrates the LCL-filter design. According to the circuit diagram in Figure 3, 50  $\mu$ F EPCOST<sup>TM</sup> capacitor has been used.  $L_1$  has been designed to be 5.2 mH and  $L_2$  to be 1 mH. A 2.5 kW 46  $\mu$ F capacitor that was found on the market has been used although  $C_f$  3.3  $\mu$ F was found via calculations. The filter resonance frequency is 810 Hz in order to not allow any overlapping problem between the system cycle and the switching frequency.

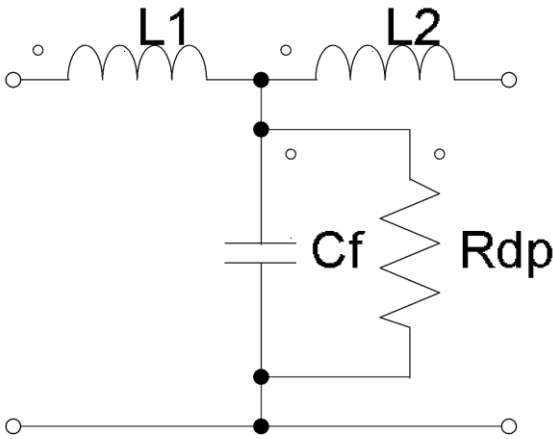


Figure 3: LCL filter circuit scheme.

### 2.3 Principle of model reference adaptive system

PMSG parameters vary depending on temperature, frequency, load conditions, and operation region. In order to eliminate the effects of parameter changes, an MRAS estimator structure that works with the proposed sensorless control method is suggested. While the rotor position error is caused by stator resistance change at low and variable speeds, with multi-parameter estimation, operation in unstable region is eliminated [37]. Also, the effects of the rotor flux linkage

variation in permanent magnet due to the temperature change are eliminated [38]. In addition to rotor flux linkage and stator resistance changes, feedforward voltage estimation method is used together with MRAS in order to eliminate the disturbance effects in position estimation. Recursive least square estimation (RLSE) is often used for determination of the parameters [39], [40]. However, the sensitivity of RLSE is not satisfactory. Furthermore, the methods such as artificial neural network (ANN), fuzzy logic, and genetic algorithms limit the dynamic performance of the system due to their intricate computations [41]. The complex estimation methods not only increase the processing time, but also decrease the reliability of the processor. Parameter estimation obtained with sliding mode observer (SMO) is not desired in critical applications due to incompatibility in response at different frequencies. Moreover, extended Kalman filter (EKF) is not recommended for PMSG systems, because it is not appropriate for multiple simultaneous estimations and comprises of complex mathematical functions [42]. Simplicity and rapid response capability of the proposed model reference adaptive system (MRAS) for PMSG is the most prominent parameter estimation method compared to other techniques [43], [44]. Predictability of stator resistance and rotor flux independently is essential for PMSG systems which require updating of generator variables independently with minimum error. The MRAS adaptation mechanism estimates slowly varying parameters based on the hyperstability theory [45]. It provides prevention of disruptive effects caused from parameter variation. The MRAS basic equation consists of a feedforward linear model and non-linear feedback components. The  $G_1$  and  $G_2$  coefficients in the  $G$  matrix ensure the feedforward linear model to be a positive and real number [43]. The non-linear block is solved according to POPOV integral equation. The proposed MRAS equations and the estimated  $dq$ -axes current equations are presented, respectively as,

$$\begin{bmatrix} \frac{di_q}{dt} \\ \frac{di_d}{dt} \end{bmatrix} = \underbrace{\begin{bmatrix} -R_s & -L_d \omega_e \\ L_q & L_q \omega_e \\ L_d \omega_e & -R_s \end{bmatrix}}_A \begin{bmatrix} i_q \\ i_d \end{bmatrix} \quad (5)$$

$$+ \underbrace{\begin{bmatrix} \frac{1}{L_q} & 0 \\ 0 & \frac{1}{L_d} \end{bmatrix}}_B \begin{bmatrix} v_q \\ v_d \end{bmatrix} + \underbrace{\begin{bmatrix} -\lambda_f \\ L_q \omega_e \\ 0 \end{bmatrix}}_C + \underbrace{\begin{bmatrix} -K\Delta v \\ -\Delta v \\ E \end{bmatrix}}_E$$

$$\begin{bmatrix} \frac{d\hat{i}_q}{dt} \\ \frac{d\hat{i}_d}{dt} \end{bmatrix} = \underbrace{\begin{bmatrix} -\hat{R}_s & -L_d \omega_e \\ L_q & L_q \omega_e \\ L_d \omega_e & -\hat{R}_s \end{bmatrix}}_{\hat{A}} \begin{bmatrix} \hat{i}_q \\ \hat{i}_d \end{bmatrix}$$

$$+ \underbrace{\begin{bmatrix} \frac{1}{L_q} & 0 \\ 0 & \frac{1}{L_d} \end{bmatrix}}_{\hat{B}} \begin{bmatrix} v_q \\ v_d \end{bmatrix} + \underbrace{\begin{bmatrix} -\hat{\lambda}_f \\ L_q \omega_e \\ 0 \end{bmatrix}}_{\hat{C}} + \underbrace{\begin{bmatrix} -K\Delta v \\ -\Delta v \\ E \end{bmatrix}}_E \quad (6)$$

$$+ \underbrace{\begin{bmatrix} G_1 & 0 \\ 0 & G_2 \end{bmatrix}}_G \begin{bmatrix} i_q - \hat{i}_q \\ i_d - \hat{i}_d \end{bmatrix}$$

where  $\hat{R}_s$  and  $\hat{\lambda}_f$  are the estimated stator resistance and rotor flux linkage, respectively which are the outputs of the adaptation model.  $\hat{R}_s$  and  $\hat{\lambda}_f$  are updated in the estimation block

in the closed loop system, as a result  $\hat{i}_q$  and  $\hat{i}_d$  currents are predicted.

$$\dot{e} = \frac{\begin{bmatrix} d(i_q - \hat{i}_q) \\ d(i_d - \hat{i}_d) \end{bmatrix}}{\frac{dt}{dt}} = \left( \begin{bmatrix} \frac{-R_s}{L_q} & \frac{-L_d}{L_q} \omega_e \\ \frac{L_q}{L_d} \omega_e & \frac{-R_s}{L_d} \end{bmatrix} + \begin{bmatrix} G_1 & 0 \\ 0 & G_2 \end{bmatrix} \right) \begin{bmatrix} i_q - \hat{i}_q \\ i_d - \hat{i}_d \end{bmatrix} + \left( \begin{bmatrix} \frac{-R_s}{L_q} & \frac{-L_d}{L_q} \omega_e \\ \frac{L_q}{L_d} \omega_e & \frac{-R_s}{L_d} \end{bmatrix} - \begin{bmatrix} \frac{-\hat{R}_s}{L_q} & \frac{-L_d}{L_q} \omega_e \\ \frac{L_q}{L_d} \omega_e & \frac{-\hat{R}_s}{L_d} \end{bmatrix} \right) \begin{bmatrix} \hat{i}_q \\ \hat{i}_d \end{bmatrix} + \left( \begin{bmatrix} -\lambda_f \\ \frac{L_q}{L_d} \omega_e \\ 0 \end{bmatrix} - \begin{bmatrix} -\hat{\lambda}_f \\ \frac{L_q}{L_d} \omega_e \\ 0 \end{bmatrix} \right) \begin{bmatrix} \hat{i}_q \\ \hat{i}_d \end{bmatrix} \quad (7)$$

In Equation (7), the errors of the MRAS current estimators are given. Selection of accurate values of  $G_1$  and  $G_2$  gains given in Equation (7) eliminate the algebraic loop problem that occurs in the simulation and experimental studies [43]. An adaptation model accomplishes the error correction. The  $G$  matrix given in Equation (7) is an observer gain matrix in which the parameters should be adjusted properly [41]. False selection of the  $G$  matrix parameters causes algebraic loops. Adaptation equations for  $\hat{R}_s$  and  $\hat{\lambda}_f$  are given respectively as

$$\hat{R}_s = -(k_{p_{res}} + \frac{k_{i_{res}}}{s})(L_s \hat{i}_d (i_d - \hat{i}_d) + \hat{i}_q (i_q - \hat{i}_q)) + \hat{R}_0 \quad (8)$$

$$\hat{\lambda}_f = -\left(k_{p_{flux}} + \frac{k_{i_{flux}}}{s}\right) \omega_e (i_q - \hat{i}_q) L_s + \hat{\lambda}_{f0} \quad (9)$$

where  $k_{p_{res}}$ ,  $k_{i_{res}}$ ,  $k_{p_{flux}}$ ,  $k_{i_{flux}}$ ,  $\hat{R}_0$ ,  $\hat{\lambda}_{f0}$  are the proportional regulator coefficient of the estimated resistance, integrator regulator coefficient of the estimated resistance, proportional regulator coefficient of the estimated rotor flux linkage, integrator regulator coefficient of the rotor flux linkage, and the estimated initial stator resistance and rotor flux linkage, respectively.

Stator resistance and rotor flux linkage estimation values in Equations (8) and (9) guarantee to give faster response than the closed loop cycle. Selection of proper regulator parameters are crucial for minimizing the steady-state error [44]. In the proposed MRAS method, a low-pass filter (LPF) is used to overcome the rise of the estimated rotor flux linkage value at low speed and at zero crossing and distortion effects caused from the stator resistance estimation. In the situations where LPF is not used at low speed, the estimation values are small and cause faulty feedforward voltage estimation values [45].

### 3 Simulation results

The proposed drive system is simulated in MATLAB/Simulink® using an electrical two-leg IGBT inverter and electrical surface-mount PM synchronous generator model from the SimPowerSystems™ toolbox in order to demonstrate the validity of the proposed speed sensorless FSTP based PMSG drive scheme. C programming like codes written in MATLAB Programming language are developed using MATLAB Function blocks without using additional toolboxes such as Embedded Coder®.

In order to show the effectiveness of the proposed method in the simulation studies, the control of the generator using the four-switch structure and the estimation of the parameters have been performed. Figure 4 shows the phase-*a* current waveform when the generator produces 110 V phase-to-phase peak voltage. Figure 5 shows the phase-*a* to phase-*b* generator voltage at transient and steady-state operation.

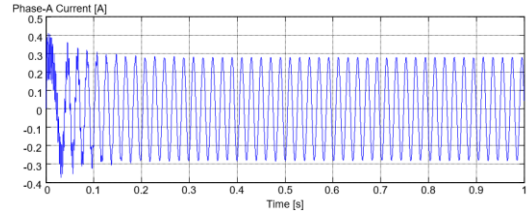


Figure 4: Phase-*a* current at transient and steady-state operation of the generator.

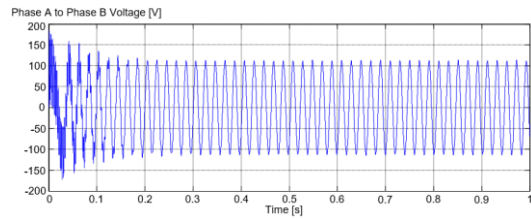


Figure 5: Phase-*a* to phase-*b* voltage at transient and steady-state operation of the generator.

Figure 6 shows the generator side duty ratios of phase-*a* and phase-*b* by using the FSTP inverter. Figure 7 shows the duty ratio in zoomed version. It is seen in Figure 7 that the proposed space vector algorithm generates expected duty cycle waveforms. Figure 8 illustrates the estimated speed and measured speed of the proposed sensorless control scheme. In Figure 9, the estimated and actual rotor positions are provided.

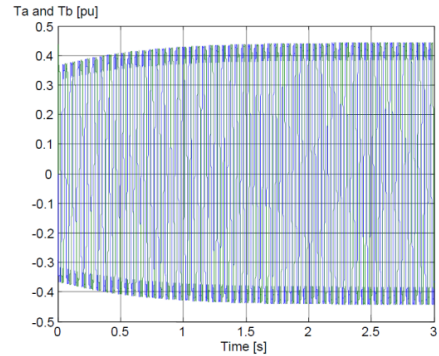


Figure 6: Duty cycle of phase-*a* and phase-*b*.

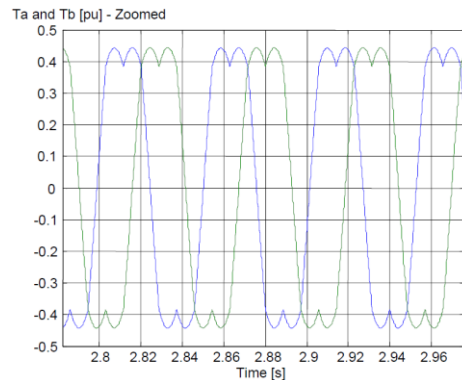


Figure 7: Duty cycle of phase-*a* and phase-*b* (zoomed).

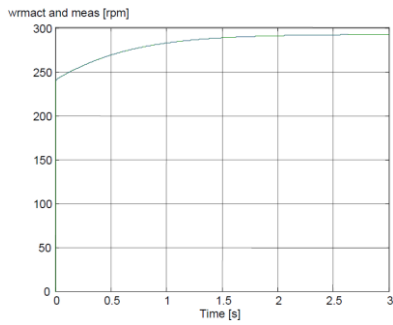


Figure 8: Actual and measured generator speeds.

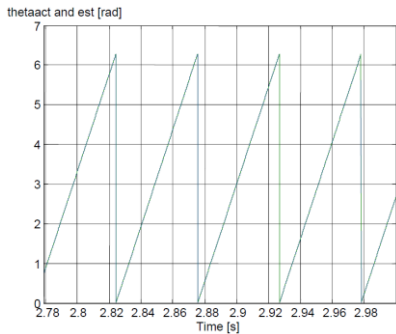


Figure 9: Actual and measured generator rotor positions.

The figures show that reasonable correlation between estimated values and actual values are achieved. In Figure 10, the initial value of the rotor flux linkage is selected incorrectly

in the simulation and then in about 0.25 s its value is converged to the original value correctly.

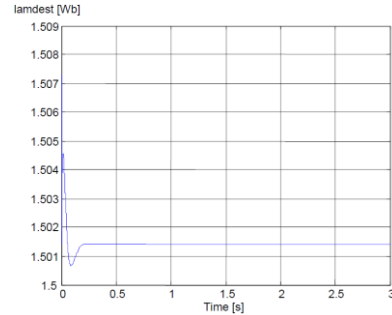


Figure 10: Estimated rotor flux linkage.

#### 4 Experimental results

To show validity of the proposed control scheme shown in Figure 11, the experimental studies are carried out for the systems shown in Figure 12 to Figure 14 under various loading conditions. A sensorless drive system for a PMSG is proposed in which stator resistance and rotor flux linkage variation are estimated. In this study, the values of stator resistance and rotor flux linkage are estimated using MRAS. However, inductance variation is neglected because the influence of the  $q$ -axis inductance is independent from the speed and position estimation, however variation of stator resistance and rotor flux linkage increase errors in the low speed region. The complete system is experimentally verified for various working conditions.

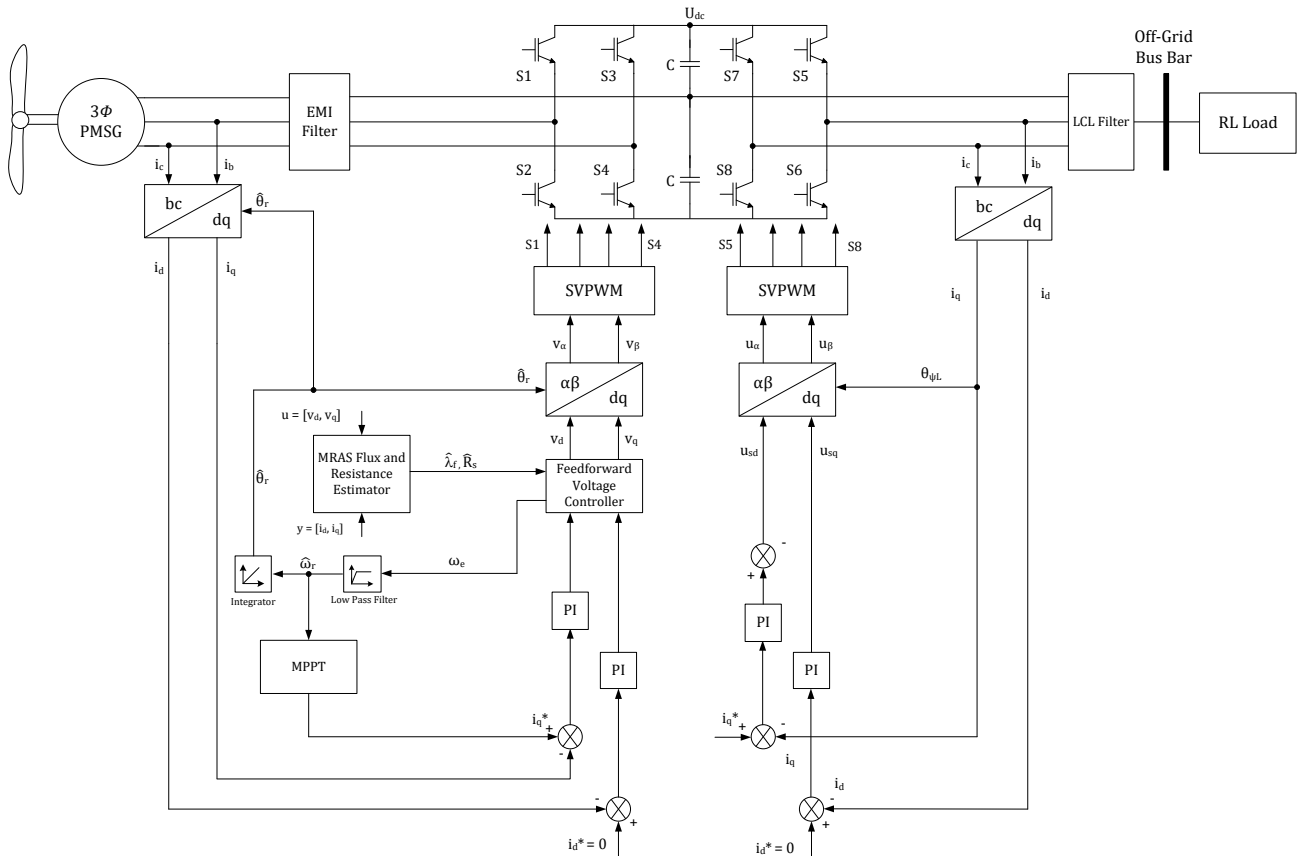


Figure 11: Overall block diagram of proposed four-switch sensorless PMSG drive model based on MRAS parameter estimation.

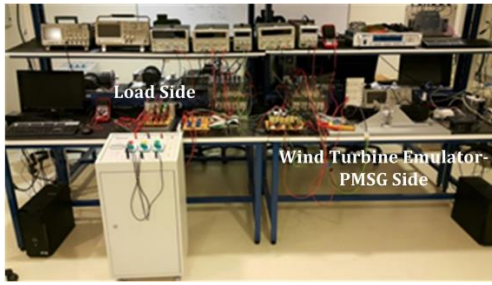


Figure 12: Experimental test-bed.

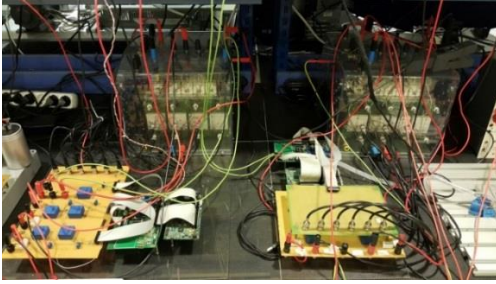


Figure 13: FSTP inverter structure (phase-*a* connected to center tap of capacitors).

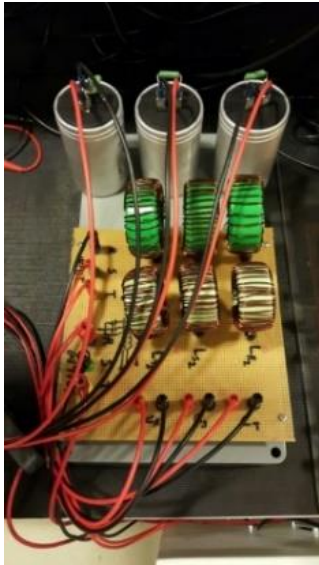


Figure 14: LCL-filter circuit.

The control algorithm is implemented on TMS320F28335 DSP and the proposed method is validated through experimental results. 3 N·m PMSM has been used via ABB® Microflex™ e150 driver to drive PMSG. Experiments have been carried out and prospected results have been obtained for the speed levels that correspond to different wind velocity levels through real-time torque control. In the system, two Semikron Semiteach modules have been modified in compliance with four-switch three-phase topology and back-to-back converter structure has been created. ALCON™ RC is used as the snubber loop. The control signals obtained through MRAS and FFVE algorithm are transmitted to the inverter/rectifier module via a signal processing card as seen in Figure 13. DC-link formed with 2200x2  $\mu$ F capacitors are connected to the rectifier and inverter inputs and outputs. For the off-grid system model, LCL output filter, seen in Figure 14, has been designed and developed.

Reaction of the system to the RL loads have been investigated by using a five-level resistive and inductive load bank. A phase-*a* center tap has been created for the FSTP via an external connection from the center tap of the two 2200x2  $\mu$ F capacitors in the experimental-bed shown in Figure 12. Output voltage of the off-grid side has been controlled through modulation index (*m*). System capabilities have been tested to obtain different values of *m*.

Figure 15 and Figure 16 show the experimental results of MRAS that is applied to the proposed sensorless method. In this system, PMSG parameters are estimated at various operating conditions. While open-loop parameter estimations are conducted during the experiments, closed-loop parameters are estimated after the estimations reach the required level and the parameters in the FFVE block have been updated. In experimental studies, initial rotor flux linkage and stator resistance estimations that are performed when stator resistance  $R_s$  is increased by 50% using MRAS are shown in Figure 15 and Figure 16, respectively.

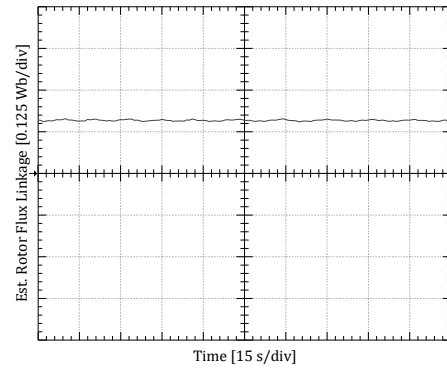


Figure 15: Estimated initial rotor flux linkage.

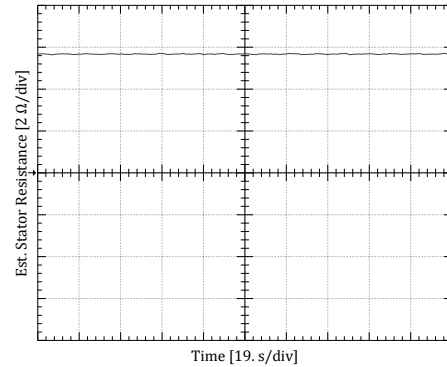


Figure 16: Estimated stator resistance when  $R_s$  is increased by 50%.

In Figure 17, phase-*a* to neutral voltage and phase-*c* to neutral voltage are represented. Phase-*a* to neutral voltage is around 60 V and phase-*c* to neutral voltage is around 53 V. Phase-*a* is the center tap point and its voltage value is around 15% more than phase-*c*. In Figure 18, phase-*a* to neutral voltage and phase-*b* to neutral voltage are shown. Phase-*a* to neutral voltage is around 60 V and phase-*b* to neutral voltage is around 53 V. While balanced voltages are observed at phase-*b* and phase-*c*, the voltage is higher at the phase connected to the center tap as it is expected. In Figure 19 and Figure 20, the stability of the proposed method for sudden load changes while *L* load being at the output of the off-grid part with five different consecutive resistor levels (22  $\Omega$  - 220  $\Omega$ ) are illustrated.

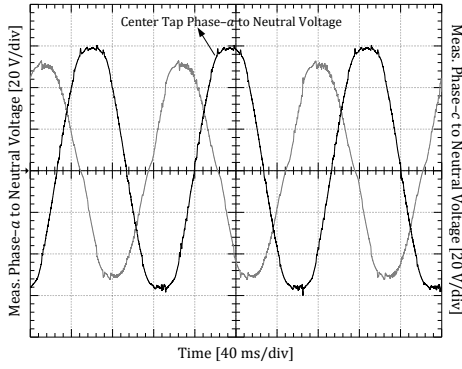


Figure 17: Phase-a to neutral and phase-c to neutral voltages.

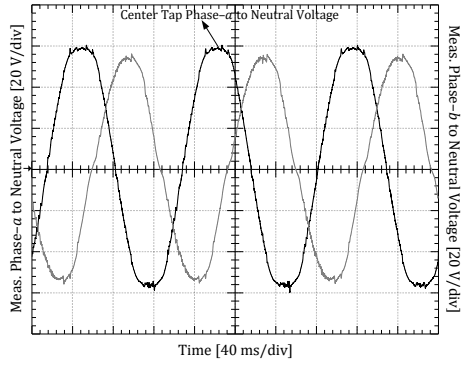


Figure 18: Phase-a to neutral and phase-b to neutral voltages.

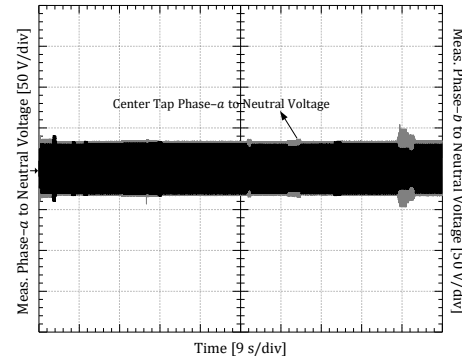


Figure 19: Meas. phase-a to neutral and phase-b to neutral voltages ( $R_{Load}$  has been changed five levels).

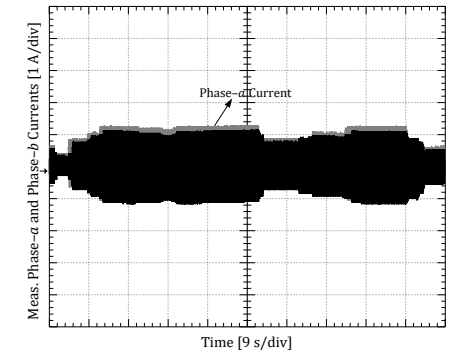


Figure 20: Meas. phase-a and phase-b currents ( $R_{Load}$  has been changed five levels).

In Figure 21, phase-a to neutral voltage is 59.2 V. PMSG has been driven to generate 100 V at the DC-link (The emulator control mode is set in the control mode). Phase-c to neutral voltage has been recorded as 54.4 V. Measurements under the

same conditions regarding phase-a and phase-b currents are represented in Figure 22. Peak value of phase-a current is 1.22 A and for phase-b current it is 1.06 A. Figure 23 shows phase-b and phase-c currents of the PMSG driven with 750 r/min. Peak value of phase-a current is 2.84 A and for phase-b current it is 2.36 A.

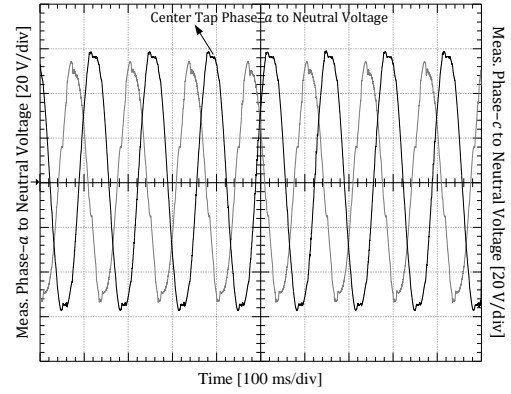


Figure 21: Meas. phase-a to neutral and phase-c to neutral voltages for  $m = 1.0$ , ( $U_{DC} = 100$  V) and ( $R_{Load} = 43 \Omega$  and  $L_{Load} = 50$  mH).

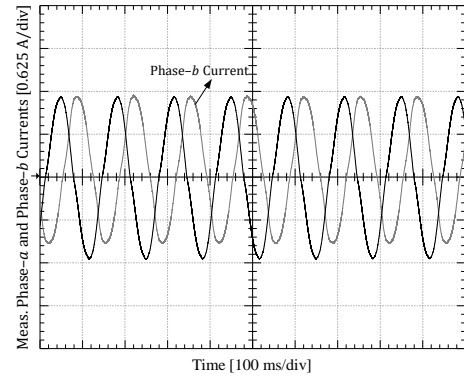


Figure 22: Meas. phase-a and phase-b currents for  $m = 1.0$ , ( $U_{DC} = 100$  V) and ( $R_{Load} = 43 \Omega$  and  $L_{Load} = 50$  mH).

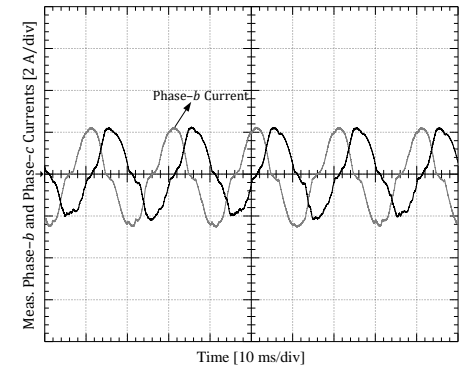


Figure 23: Meas. phase-b and phase-c currents for  $m = 0.4$ , ( $U_{DC} = 100$  V) and ( $R_{Load} = 43 \Omega$  and  $L_{Load} = 50$  mH).

In Figure 24, the peak value of phase-c current under the same conditions have been measured as 2.36 A. Unbalance between phases in FSTP controlled PMSG have been measured as 15% for voltages and 20% for currents. Figure 25 illustrates phase-a and phase-b currents of the PMSG driven with 500 r/min. Peak value of phase-a current is 2.68 A and for phase-b current it is 2.36 A. In Figure 26, the peak value of phase-c current under the same conditions has been measured as 2.12 A.

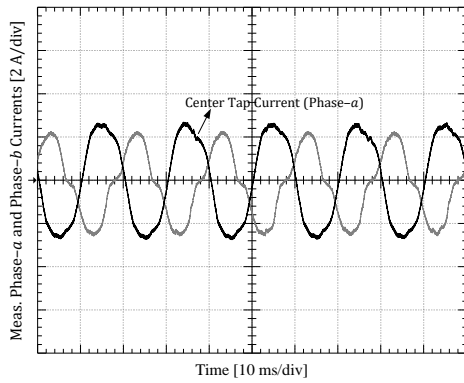


Figure 24: Meas. phase-*a* and phase-*b* currents for  $m = 1.0$ , ( $U_{DC} = 100\text{ V}$ ) and ( $R_{Load} = 43\ \Omega$  and  $L_{Load} = 50\text{ mH}$ ).

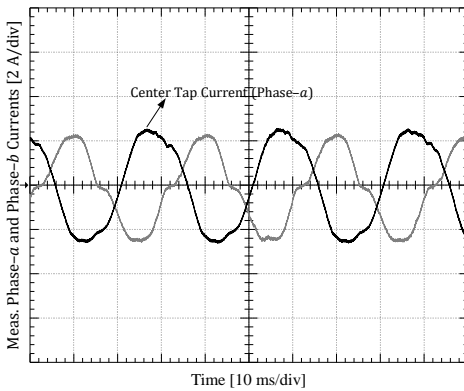


Figure 25: Meas. phase-*a* and phase-*b* currents for  $m = 0.5$ , ( $U_{DC} = 100\text{ V}$ ) and ( $R_{Load} = 43\ \Omega$  and  $L_{Load} = 50\text{ mH}$ ).

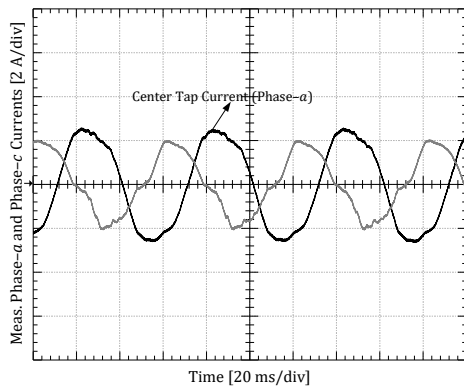


Figure 26: Meas. phase-*a* and phase-*c* currents for  $m = 0.5$ , ( $U_{DC} = 100\text{ V}$ ) and ( $R_{Load} = 43\ \Omega$  and  $L_{Load} = 50\text{ mH}$ ).

In the control system, FSTPI may cause instability due to the unbalancing in the capacitors that create voltage unbalancing in the low speed region of sensorless FSTPI drive which relies on back-EMF sensing. In addition, since there is no zero-voltage vector as in SSTPI, there exist more harmonics as well as oscillations in currents and voltages in FSTPI. Under insufficient DC bus voltage conditions, the targeted power level cannot be reached due to the ratio of the voltages between SSTPI and FSTPI which is  $1/3$  to  $2/3$  and the low speed operation of FSTPI with the proposed method fails. Moreover, even if the DC bus voltage is increased, serious voltage and current oscillations and harmonics in the system are observed and the motor insulations might break. Normally, DC voltage in FSTP should be  $C_1 = C_2$  at ideal conditions, however in the real

system it becomes  $C_1 \neq C_2$  during steady-state operation. Therefore, based on the measurement time, differences are observed between peak values of phase-*a* and -*b* currents.

Moreover, because the dead-time effect is not compensated, the phase current waveform exhibits some additional distortion especially at zero crossings and at around positive and negative peaks.

Measurements show that imbalance between phases in FSTP controlled PMSG is 15% for phase-*a* and phase-*b*, 10% for the phase-*b* and phase-*c*, and 25% for the phase-*a* and phase-*c* voltages. It can be observed that the lower the speed level under PMSG control, the more the unbalance condition between the phases occurs. 200 r/min speed level has been achieved by using the proposed method based on multi-parameter estimation. Experimental results show that the distortion effects of stator resistance and rotor flux linkage dominate at low speed position estimation. This speed value corresponds to 0.06 p.u. at the PMSG having 3000 r/min rated speed. Results for grid/load output and THD analysis are examined separately for LCL filter output and LCL filter input cases. The THD of the phase-*a* to phase-*b* voltage of the four switch grid/load side LCL filter input is around 51%. The THD of the phase-*a* to phase-*b* voltage of the four switch grid/load side LCL filter output is around 6.6%. The validity of the designed filter and selected values is confirmed from the waveforms whose THD value is around  $<7\%$ .

## 5 Conclusions

While macro-scale wind turbines are solving problems at industrial and high-power levels, participation of individual users into energy production is possible with micro-scale wind turbines. Especially, rural zones without electric energy, base stations, highways and individual uses are said to be application areas for micro-scale energy production. It can be easily predicted that the small powerful energy production can be rapidly increased with integration of smart grid. The control of gearless Permanent Magnet Synchronous Generator (PMSG) along with load side inverter control in this work are performed using a full-rating, bi-directional, two-level, back-to-back voltage source rectifier/inverter with a total of 8 switches for the variable speed wind turbine. In the proposed four-switch PMSG control method, MRAS rotor flux linkage and stator resistance estimator is used to correct changes in the flux and stator resistance values in PMSG drive. It is proved with this study that the inclusion of a simple, effective and low-cost position sensorless control enhanced with MRAS multi-parameter estimation in the generator side show that renewable wind energy system can be a viable distributed green energy solution for rural areas.

## 6 References

- [1] American Wind Energy Turbine Market Report. "AWEA Small Wind Turbine Global Market Study". American Wind Energy Association, 2010.
- [2] U.S. Department of Energy. "2014 Distributed Wind Market Report". U.S. Department of Energy, 2014.
- [3] Smith J, Huskey A, Jager D, Hur J. "Wind Turbine Generator System Power Performance Test Report for The EW50 Wind Turbine Simulation Model of Wind Turbine". 2011.
- [4] Renewable UK. "Small and Medium Wind UK Market Report", 2013.

- [5] Dasgupta S, Mohan SN, Sahoo SK, Panda SK. "Application of four-switch-based three-phase grid-connected inverter to connect renewable energy source to a generalized unbalanced microgrid system". *IEEE Transactions on Industrial Electronics*, 60(3), 1204-1215, 2013.
- [6] Zhao Y, Wei C, Zhang Z, Qiao W. "A review on position/speed sensorless control for permanent-magnet synchronous machine-based wind energy conversion systems". *IEEE Journal of Emerging and Selected Topics in Power Electronics*, 1(4), 203-216, 2013.
- [7] Parviainen A, Pyrhonen J, and Kontkanen P. "Axial flux permanent magnet generator with concentrated winding for small wind power applications". *IEEE International Electric Machines and Drives Conference*, San Antonio, TX, USA, 15-18 May 2005.
- [8] Bumby JR, Stannard N, Dominy J, McLeod N. "A permanent magnet generator for small scale wind and water turbines". *IEEE International Conference on Electrical Machines*, Coimbra, Portugal, 6-9 September 2008.
- [9] Andriollo M, De Bortoli M, Martinelli G, Morini A, Tortella A. "Permanent magnet axial flux disc generator for small wind turbines". *IEEE International Conference on Electrical Machines*, Vilamoura, Portugal, 6-9 September 2008.
- [10] Olano A, Moreno V, Molina J, Zubia I. "Design and construction of an outer-rotor PM synchronous generator for small wind turbines; comparing real results with those of FE model". *IEEE International Conference on Electrical Machines*, Vilamoura, Portugal, 6-9 September 2008.
- [11] Haraguchi H, Morimoto S, Sanada M. "Suitable design of a PMSG for a small-scale wind power generator". *International Conference on Electrical Machines and Systems*, Tokyo, Japan, 15-18 November 2009.
- [12] Yan J, Lin H, Feng Y, Guo X, Huang Y, Zhu ZQ. "Improved sliding mode model reference adaptive system speed observer for fuzzy control of direct-drive permanent magnet synchronous generator wind power generation system". *IET Renewable Power Generation*, 7(1), 28-35, 2013.
- [13] Zhang Z, Zhao Y, Qiao W, Qu L. "A space-vector-modulated sensorless direct-torque control for direct-drive PMSG wind turbines". *IEEE Transaction on Industry Applications*, 50(4), 2331-2341, 2014.
- [14] Tan K, Islam S. "Optimum control strategies in energy conversion of PMSG wind turbine system without mechanical sensors". *IEEE Transaction on Energy Conversion*, 19(2), 392-399, 2004.
- [15] Okuyama Y, Fujimoto T, Matsui N, Kubota T. "A high performance speed control scheme of induction motor without speed and voltage sensors". *IEEE Industry Applications Society Annual Meeting*, Denver, Colorado, USA, 28 September-3 October 1986.
- [16] Seok JK, Lee JK, Lee DC. "Sensorless speed control of nonsalient permanent-magnet synchronous motor using rotor-position-tracking PI controller". *IEEE Transaction on Industrial Electronics*, 53(2), 399-405, 2006.
- [17] Yang S, Guo L, Qi L, Chang L, Zhang X. "A parameter-robust sliding mode observer for speed sensorless torque control of PMSG in wind power generation system". *IEEE Canadian Conference on Electrical and Computer Engineering*, Halifax, Nova Scotia, Canada, 3-6 May 2015.
- [18] Ichikawa S, Tomita M, Doki S, Okuma S. "Sensorless control of permanent-magnet synchronous motors using online parameter identification based on system identification theory". *IEEE Transaction on Industrial Electronics*, 53(2), 363-372, 2006.
- [19] Xiao X, Chen C, Zhang M. "Dynamic permanent magnet flux estimation of permanent magnet synchronous machines". *IEEE Transaction on Applied Superconductivity*, 20(3), 1085-1088, 2010.
- [20] Kerkman RJ, Skibinski GL, Schlegel DW. "A.C. drives; Year 2000 and beyond". *IEEE Applied Power Electronics Conference and Exposition*, Dallas, TX, USA, 14-18 March 1999.
- [21] Chan TF, Wang W, Borsje P, Wong YK, Ho SL. "Sensorless permanent-magnet synchronous motor drive using a reduced-order rotor flux observer". *IET Electric Power Applications*, 2(2), 88-98, 2008.
- [22] Cacciato A, Scarcella M, Scelba G, Bille G, Costanzo SM, Cucuccio D. "Comparison of low-cost-implementation sensorless schemes in vector controlled adjustable speed drives". *IEEE International Symposium on Power Electronics, Electrical Drives, Automation and Motion*, Ischia, Italy, 11-13 June 2008.
- [23] Chen Z, Guerrero JM, Blaabjerg F. "A review of the state of the art of power electronics for wind turbines". *IEEE Transaction on Power Electronics*, 24(8), 1859-1875, 2009.
- [24] Jacobina CB, da Silva ERC, Lima AMN, Ribeiro RLA. "Induction generator static systems with a reduced number of components". *IEEE Industry Applications Society Annual Meeting*, San Diego, CA, USA, 6-10 October 1996.
- [25] Raju AB, Chatterjee K, Fernandes BG. "A simple maximum power point tracker for grid connected variable speed wind energy conversion system with reduced switch count power converters". *IEEE 34th Annual Power Electronics Specialist Conference*, Acapulco, Mexico, 15-19 June 2003.
- [26] Dos Santos EC, Jacobina CB, Rocha N, Dias JAA, Correa MBR. "Single-phase to three-phase four-leg converter applied to distributed generation system". *IET Power Electronics*, 3(6), 892-903, 2010.
- [27] Baktash A, Jalilian A, Vahedi A. "Direct power control of reduced switch active filters". *IEEE 14th International Conference on Harmonics and Quality of Power*, Bergamo, Italy, 26-29 September 2010.
- [28] Bose BK. *Power Electronics and Variable Frequency Drives-Technology and Applications*. 1<sup>st</sup> ed. Piscataway, New Jersey, USA, IEEE Press, 1997.
- [29] Krishnan R. *Permanent Magnet Synchronous and Brushless DC Motor Drives*. 1<sup>st</sup> ed. Boca Raton, Florida, USA, CRC Press, 2009.
- [30] Pillay P, Krishnan R. "Modeling, simulation and analysis of permanent-magnet motor drives, Part. I: The permanent-magnet synchronous motor drive". *IEEE Transaction on Industry Applications*, 25(2), 265-273, 1989.
- [31] Reznik A, Simões MG, Al-Durra A, Muyeen SM. "LCL filter design and performance analysis for small wind turbine systems". *IEEE Power Electronics and Machines in Wind Applications*, Denver, CO, USA, 16-18 July 2012.
- [32] Beres RN, Wang X, Liserre M, Blaabjerg F, Bak CL. "A review of passive power filters for three-phase grid Connected voltage-source converters". *IEEE Journal of Emerging and Selected Topics in Power Electronics*, 4(1), 54-69, 2015.

- [33] Araujo SV, Engler A, Sahan B, Antunes FLM. "LCL filter design for grid-connected NPC inverters in offshore wind turbines". *7<sup>th</sup> International Conference on Power Electronics*, Daegu, South Korea, 22-26 October 2007.
- [34] Ahmed KH, Finney SJ, Williams BW. "Passive filter design for three-phase inverter interfacing in distributed generation". *Compatibility in Power Electronics*, Gdansk, Poland, 29 May-1 June 2007.
- [35] Reznik A, Simões MG, Al-Durra A, Muyeen SM. "LCL filter design and performance analysis for grid-interconnected systems". *IEEE Transaction on Industry Applications*, 50(2), 1225-1232, 2014.
- [36] Zabaleta M, Burguete E, Madariaga D, Zubimendi I, Zubiaga M, Larrazabal I. "LCL grid filter design of a multimewatt medium-voltage converter for offshore wind turbine using SHEPWM modulation". *IEEE Transaction on Power Electronics*, 31(3), 1993-2001, 2016.
- [37] Nahid-Mobarakeh B, Meibody-Tabar F, Sargos FM. "Mechanical sensorless control of PMSM with online estimation of stator resistance". *IEEE Transaction on Industry Applications*, 40(2), 457-471, 2004.
- [38] Stumberger B, Stumberger G, Dolinar D, Hamler A, Trlep M. "Evaluation of saturation and cross-magnetization effects in interior permanent-magnet synchronous motor". *IEEE Transaction on Industry Applications*, 39(5), 1264-1271, 2003.
- [39] Ramakrishnan R, Islam R, Islam M, Sebastian T. "Real time estimation of parameters for controlling and monitoring permanent magnet synchronous motors". *International Conference on Electrical Machines and Systems*, Miami, FL, USA, 3-6 May 2009.
- [40] Underwood SJ, Husain I. "Online parameter estimation and adaptive control of permanent-magnet synchronous machines". *IEEE Transactions on Industrial Electronics*, 57(7), 2435-2443, 2010.
- [41] Liu K, Zhu ZQ, Stone DA. "Parameter estimation for condition monitoring of PMSM stator winding and rotor permanent magnets". *IEEE Transaction on Industrial Electronics*, 60(12), 5902-5913, 2013.
- [42] Benadja M, Chandra A. "Adaptive sensorless control of PMSGs-based offshore wind farm and VSC-HVDC stations". *IEEE Journal of Emerging and Selected Topics in Power Electronics*, 3(4), 918-931, 2015.
- [43] Eskola M, Tuusa H. "Comparison of MRAS and novel simple method for position estimation in PMSM drives". *IEEE 34<sup>th</sup> Annual Power Electronics Specialist Conference*, Acapulco, Mexico, 15-19 June 2003.
- [44] Baik I, Kim KH, Young MJ. "Robust nonlinear speed control of PM synchronous motor using boundary layer integral sliding mode control technique". *IEEE Transaction on Control Systems Technology*, 8(1), 47-54, 2002.
- [45] Boileau T, Nahid-Mobarakeh B, Meibody-Tabar F. "On-line identification of PMSM parameters: Model-reference vs EKF". *IEEE Industry Applications Society Annual Meeting*, Edmonton, AB, Canada, 5-9 October 2008.